Self-Absorption in Resonance Raman and Rayleigh Scattering: A Numerical Solution

MICHAEL LUDWIG and SANFORD A. ASHER*
Department of Chemistry, University of Pittsburgh, Pittsburgh, Pennsylvania 15260

We have numerically calculated the parameters necessary to correct Raman intensities for self-absorption for Raman measurements utilizing a 90° scattering geometry and a cylindrical capillary sample cell. We display curves that can be used to extract these parameters for any sample absorbances at the incident laser excitation wavelength and the Raman scattered wavelength. These results make it possible, for the first time, to quantitatively utilize resonance Raman spectroscopy to determine concentrations of analytes. These parameters can also be used to numerically correct resonance Raman excitation profile measurements for self-absorption. These results clearly illustrate the dependence of spectral signal-to-noise ratios and spectral detection limits upon signal attenuation due to self-absorption.

Index Headings: **Raman spectroscopy, instrumentation; absorption.**

INTRODUCTION

Quantitative analytical applications of resonance Raman spectroscopy are hindered by the experimental difficulties encountered in measuring the intrinsic Raman intensities that are proportional to the concentrations of analytes.[1,2] Excitation of absorbing samples results in attenuation of both the exciting light and the Raman scattered light. If the sample absorbance varies with wavelength, the individual Raman bands will be differently attenuated. In this work we develop a model for a typical Raman experimental situation and calculate the effect of sample self-absorption on the observed Raman intensities.

The degree to which self-absorption affects a resonance Raman measurement depends on the magnitude and band shape of the resonant absorption spectrum and the geometry of the scattering experiment. Earlier self-absorption studies examined the effects of self-absorption on Raman intensity measurements made with arc lamp excitation sources.[1,3,4] More recently, simplified models were used to predict optimal sample concentrations for laser excitation,[5-7] and a 180° backscattering geometry was examined[8] qualitatively in order to develop approximate expressions to correct resonance Raman intensities for self-absorbance.[9,10]

In spite of all of this work, self-absorption has not yet been accurately or quantitatively modeled for cases which reflect typical experimental conditions (where it is recognized that the exciting beam has a finite extent and scattered light is collected over a large solid angle). This is because it is difficult, if not impossible, to analytically solve the resulting expressions. In this work, we numerically calculate the magnitude of attentuation of the Raman and Rayleigh intensities by self-absorption. We theoretically determine correction parameters which can be used with experimental data to calculate intrinsic Raman intensities. We also quantitatively examine how self-absorption biases measured Raman and Rayleigh excitation profiles under typical experimental conditions. Finally, we examine the effect of self-absorption on spectral signal-to-noise ratios and Raman detection limits. Our study quantitatively calculates the magnitude of self-absorption for a particular sample geometry. However, we caution that the depth of focus of the collection optic (transfer function) is an important determinant of the exact sample volume in a Raman measurement. The results calculated here give the maximum likely self-absorption correction function. The calculation of the exact self-absorption correction for a particular spectrometer requires specification of the collection optic transfer function.

THEORY

Our self-absorption calculation utilizes a 90° Raman scattering geometry from a cylindrical sample, as shown in Fig. 1. In the absence of absorption, the total Raman-scattered intensity, I_T from a given volume element within a capillary is proportional to the incident beam intensity, I_0 (photons/cm^2 s) and the number of scattering species, N, within the volume element:[11]

$$I_T = \sigma I_0 N \tag{1}$$

where σ is the total Raman cross section of the band integrated over the entire 4π solid angle. The observed intensity of Raman scattering, I_{TO}, from each volume element V collected within solid angle $d\Omega_v$, is:

$$I_{TO} = I_T \frac{d\Omega_v}{4\pi} . \tag{2}$$

We assume a 100% efficiency for detection of the collected light. The magnitude of self-absorption attenuation differs between volume elements because different pathlengths exist for excitation into each volume element, and because different pathlengths exist for transmittance of the scattered light out of each volume element; the transmittance decreases exponentially with the pathlength. Furthermore, each volume element within the capillary projects a different solid angle onto the collection optic. Thus, each volume element will contribute differently to the total Raman intensity. Figure 2A shows the intensity attenuation of the excitation beam within a 1.0-mm-diameter cylindrical sample with an absorbance of 10/cm that occurs for a collimated incident laser beam which has a constant cross sectional intensity. Figure 2B similarly shows the excitation intensity attenuation for a collimated laser beam which has a Gaussian cross sectional intensity (sigma = 0.28 mm). Figure 2A indicates that the intensity is high at the capillary edges. Thus, volume elements close to the edge facing the collection optic will selectively contribute to the observed Raman intensities. In contrast, most of the excitation

Received 31 May 1988.
* Author to whom correspondence should be sent.

0003-7028/88/4208-1458$2.00/0

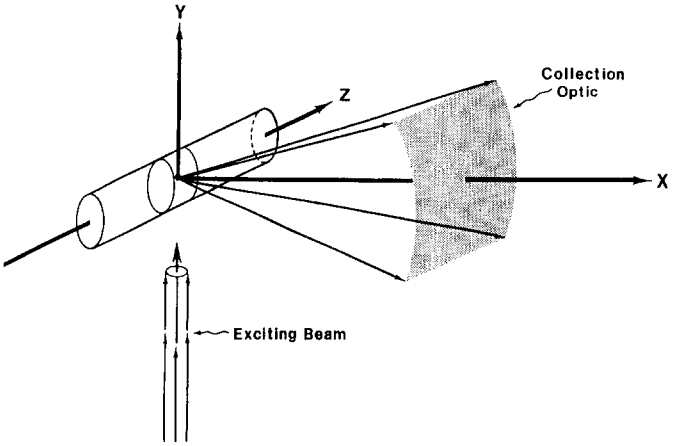

FIG. 1. The sample geometry for 90° Raman scattering from a cylindrical sample.

intensity remains in the center of the capillary for the Gaussian beam (Fig. 2B). Thus, volume elements within the lower bottom edge of the capillary selectively contribute to the observed Raman intensities. Figures 2A and 2B clearly indicate that the incident beam intensity profile is important in determining the selection of sample volume elements that contribute to the observed Raman intensities.

The intensity incident onto particular volume elements illuminated by the collimated laser beam of constant cross sectional intensity is calculated with the use of the geometry shown in Fig. 3. The center of the capillary is the origin of the cylindrical coordinate system. The intensity at each infinitesimally small volume element, V, within the capillary is:

$$I_V = I_0(r)e^{-2.303c\epsilon_0\ell} \tag{3}$$

where $I_0(r)$ is the intensity of the incident laser beam at the distance r from the beam axis. For a beam of constant cross sectional intensity, $I_0(r)$ is independent of r. The concentration of the absorbing species is given by c; ϵ_0 is the molar absorptivity at the excitation wavelength; and ℓ is the pathlength of the beam through the capillary to volume element V. The intensity at V is:

$$I_V = I_0(r)e^{-2.303c\epsilon_0(\rho_V \sin\Phi_v + \sqrt{\rho_0^2 - \rho_V^2\cos^2\Phi_V})} \tag{4}$$

where ρ_0 is the capillary radius, and ρ_V, Φ_V, Z_V are the cylindrical coordinates of volume element V. We neglect refraction of the incident beam as it passes through the air/sample interface (*vide infra*).

The absorption of the scattered light is most easily treated after transformation to a spherical polar coordinate system. Calculating the Cartesian coordinates (X_V, Y_V, Z_V) of V from its cylindrical coordinates:

$$\begin{aligned} X_V &= \rho_V\cos\Phi_V \\ Y_V &= \rho_V\sin\Phi_V \\ Z_V &= Z_V \end{aligned} \tag{5}$$

and the spherical polar coordinates (P_V, θ_V, Φ_V):

$$\begin{aligned} P_V &= (X_V^2 + Y_V^2 + Z_V^2)^{1/2} \\ \theta_V &= \cos^{-1}\left(\frac{Z_V}{\sqrt{X_V^2 + Y_V^2 + Z_V^2}}\right) \\ \Phi_V &= \tan^{-1}\left(\frac{Y_V}{X_V}\right). \end{aligned} \tag{6}$$

Equation 4 determines the excitation intensity at V. It then remains to calculate Ω_V, the solid angle of collection for each volume element, and to calculate the pathlength for each ray of Raman-scattered light that leaves the volume element and is collected by the collection optic. The calculated intensities from all rays are summed for each volume element, and all the volume elements are summed over the entire illuminated sample volume to generate the self-absorption correction factor.

The collection optic acceptance cone limits are calculated in the Cartesian coordinate system, as shown in Fig. 4. The angular acceptance cone limits (α, β, γ, and χ) are calculated as:

$$\begin{aligned} \alpha &= \tan^{-1}\left(\frac{A - Y_V}{D - X_V}\right) \\ \beta &= -\tan^{-1}\left(\frac{B + Y_V}{D - X_V}\right) \\ \chi &= \frac{\pi}{2} + \tan^{-1}\left(\frac{R + Z_V}{D - X_V}\right) \\ \gamma &= \frac{\pi}{2} - \tan^{-1}\left(\frac{L - Z_V}{D - X_V}\right) \end{aligned} \tag{7}$$

where D is the distance from the center of the capillary to the center of the rectangular collection optic. A and B are the distances from the center of the collection optic to the edges parallel to the capillary axis, while L and R are the distances from the center of the optic to the edges perpendicular to the capillary axis.

A rectangular collection optic was chosen for calculational convenience and also because it mimics the shape of the ellipsoidal collection mirror we use for Raman measurements.[12] The calculation assumes that for each volume element V, angles α, β, γ, and χ can be defined, and the sets α, β and γ, χ are independent of one another. This approximation is extremely useful because it dramatically decreases the calculation time, by approximating the projection of a square into a sphere to be a square. In the calculation here, this approximation effectively fattens slightly and elongates the corners of the collection optic. A negligible error results from this approximation for the sample geometry considered, since the size (6 cm) of the square is less than its distance (10 cm) from the volume element V; the effective collection $f/\#$ is ~0.7.

We assume that the Raman scattering is isotropic. Thus, to calculate the intensity of the observed Raman-scattered light from V impinging on the collection optic, we create on the surface of a sphere centered about V a net of equal small solid angles. Each infinitesimally small solid angle on the sphere surface corresponds to a ray of

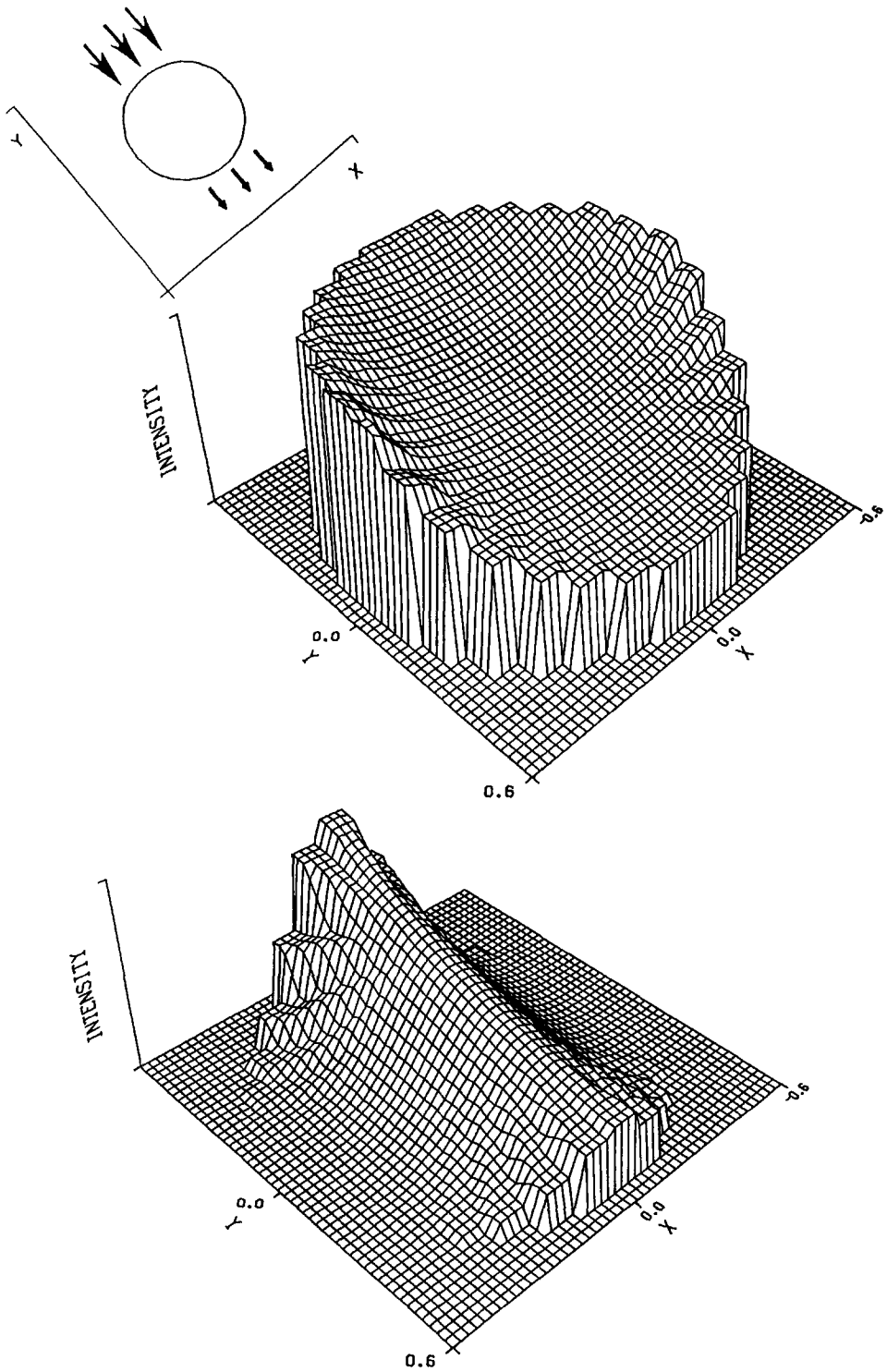

FIG. 2. Intensity profiles of an excitation beam passing into a 1-mm-diameter cylindrical sample which has an absorbance of 10/cm. The beam illuminates the capillary along the Y-axis. (A) The intensity profile for a collimated laser beam of constant cross sectional intensity. (B) Intensity profile for a collimated laser beam with a Gaussian cross sectional intensity (sigma = 0.28 mm).

Raman-scattered light leaving V. The resulting spherical polar coordinate systems are shown in Fig. 5. The origin of the unprimed system occurs at the center of the capillary, while the origin of the primed system occurs at volume element V. The net of solid angles must be sufficiently fine for the calculation to accurately converge. To create this net of equal solid angles we increment Φ and use the recursion formula given by Eq. 8 to determine the next value of angle θ:

$$\cos \theta_2 = \cos \theta_1 - \frac{\Delta\Omega}{\Delta\Phi} \tag{8}$$

where θ_1 is the previously calculated value of θ and $\Delta\Phi$ and $\Delta\Omega$ are the calculational increments chosen for Φ_V and Ω_V. θ is limited to values between 0 and π. Scattering occurs for the set of rays defined by θ and Φ within the limits imposed by angles α, β, γ, and χ. We utilized a net with a solid angle increment of 3.6×10^{-5} sr.

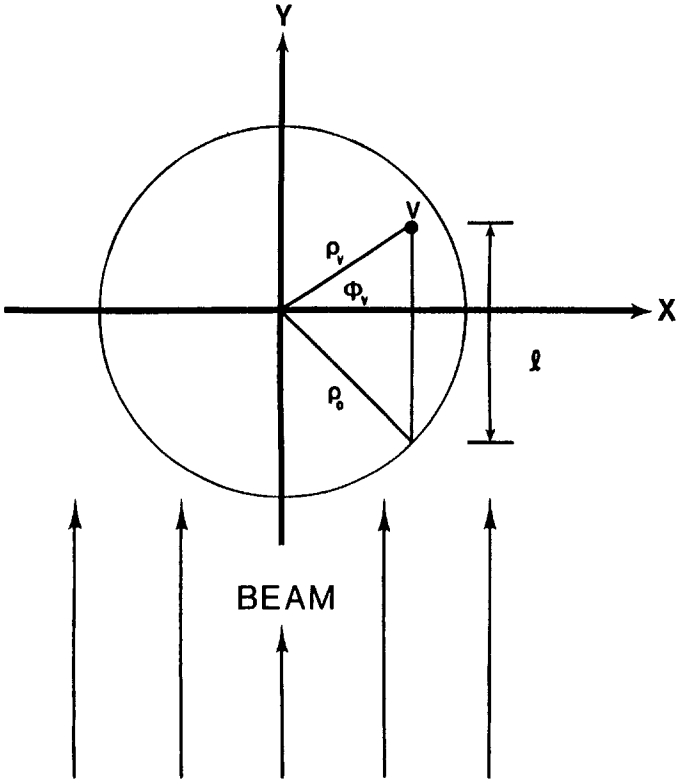

FIG. 3. Geometry for calculating the intensity incident at a given point in a capillary illuminated by a laser beam propagating along the Y-direction and perpendicular to the capillary axis. The capillary radius is ρ_0. The coordinates of the volume element are P_V, Φ_V, and Z_V in a cylindrical coordinate system with the origin at the capillary center. The pathlength of the beam through the capillary to the volume element V is given by ℓ.

Figure 5 shows the geometry used to calculate the pathlength out of the capillary taken by a ray scattered from V along an angle θ'_P and Φ'_P. The expression:

$$X_p^2 + Y_p^2 = \rho_0^2 \tag{9}$$

defines the cylindrical coordinates, measured from the

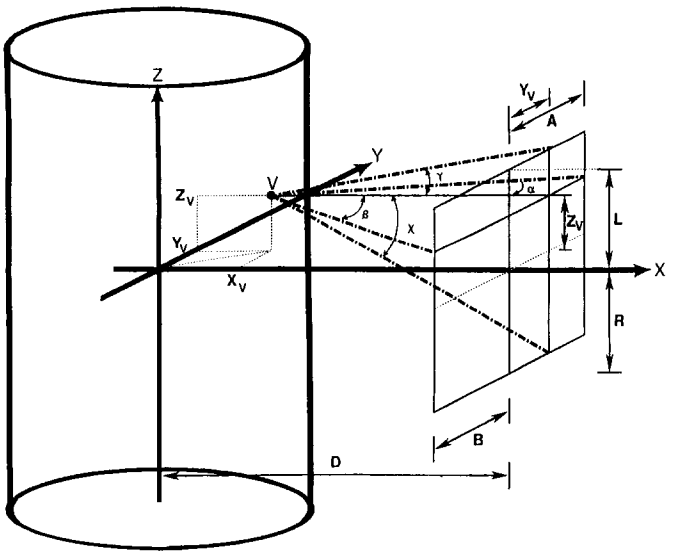

FIG. 4. (A) The geometry for 90° scattering. The capillary is situated, by a distance, D, from the collection optic. A, B, L, and R label the edges of the collection optic. X_V, Y_V, and Z_V are the Cartesian coordinates of volume element V.

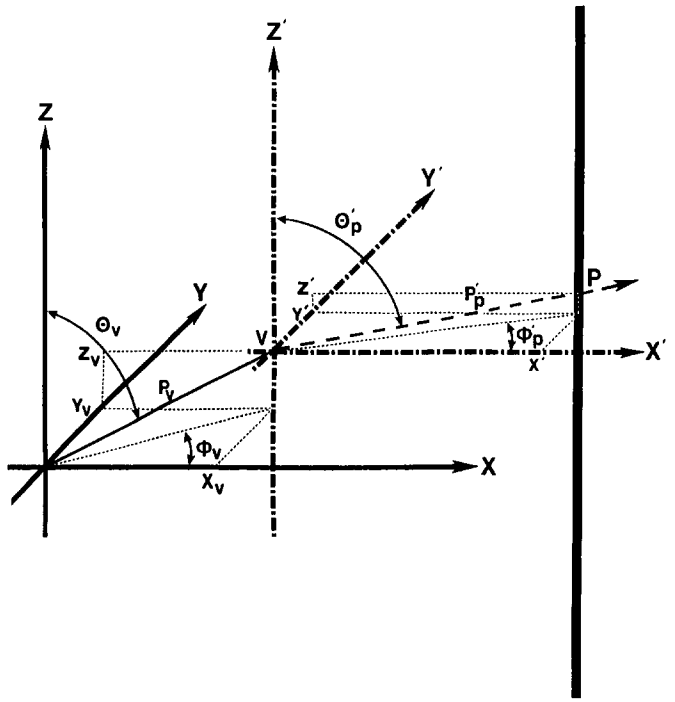

FIG. 5. Relationship between the spherical polar coordinate systems originating at volume element V and that at the center of the capillary. The pathlength between V and point P on the capillary wall is calculated along the ray defined by angles θ'_P and Φ'_P.

center of the capillary, of point P where the ray exits the capillary. Translation to the coordinate system centered at V gives:

$$(X_V + X'_p)^2 + (Y_V + Y'_p)^2 = \rho_0^2 \tag{10}$$

where X'_p and Y'_p represent the Cartesian coordinates of P measured from V, and X_V and Y_V are the coordinates of V. Solving for Y'_p gives:

$$Y'_p = (\rho_0^2 - (X_V + X'_p)^2)^{1/2} - Y_V. \tag{11}$$

Transformation to the spherical polar coordinate system centered at V gives:

$$\begin{aligned} P'_p \sin\theta'_p \sin\Phi'_p = [&\rho_0^2 - (P_V \sin\theta_V \cos\Phi_V \\ &+ P'_p \sin\theta'_p \cos\Phi'_p)^2]^{1/2} \\ &- P_V \sin\theta_V \sin\Phi_V \end{aligned} \tag{12}$$

where P'_P, θ'_P, and Φ'_P locate P in the spherical polar system centered at V, and P_V, θ_V, and Φ_V are the coordinates of V in the spherical polar coordinate system centered at the capillary center. Solving for P'_p, the distance between V and P, gives:

$$\begin{aligned} P'_p = \{&[\rho_0^2 - P_V^2 \sin^2\theta_V \\ &+ (P_V \sin\theta_V (\sin\Phi'_p \sin\Phi_V + \cos\Phi'_p \cos\Phi_V)^2]^{1/2} \\ &- P_V \sin\theta_V (\sin\Phi_p' \sin\Phi_V \\ &+ \cos\Phi_p' \cos\Phi_V)\} / \sin\theta_p'. \end{aligned} \tag{13}$$

The intensity of Raman or Rayleigh scattered light decreases exponentially along this pathlength.

The Raman-scattered intensity observed, I_{obs}, is calculated by summing the contributions from all the rays and over all of the illuminated volume elements, recognizing that solid angle of light collection varies between volume elements:

TABLE I. The dependence of R upon the number of volume elements and the absorbance at the excitation wavelength, A_0, and analyte Raman band wavelength, A_a. The capillary diameter was 1.0 mm. See text for details of calculation.

Volume elements	Total rays	R $A_0 = 10.0$ $A_a = 2.0$	$A_0 = 20.0$ $A_a = 4.0$	$A_0 = 100.0$ $A_a = 20.0$
1	9207	3.049	9.297	69,451.950
8	73,359	2.430	5.453	1136.422
27	247,401	2.501	4.697	41.726
64	586,410	2.492	4.800	64.459
125	1,145,265	2.467	4.526	30.447
216	1,978,647	2.441	4.446	29.275
343	3,141,996	2.456	4.480	27.474
512	4,690,488	2.462	4.509	29.722
729	6,677,979	2.451	4.460	26.225
1000	9,160,866	2.445	4.434	25.891
1331	12,192,972	2.448	4.449	25.565
1728	15,829,374	2.452	4.465	26.378

$$I_{obs} = \sigma N \sum_V \sum_{\Delta\Omega} I_V e^{-2.303 P'_{PV}(\Delta\Omega)\epsilon_a c} \quad (14)$$

where ϵ_a is the molar absorptivity at the scattered wavelength. P'_{PV} $(\Delta\Omega)$ is the pathlength of the scattered ray associated with the incremental solid angle $\Delta\Omega$ out of the capillary from volume element V.

We define a parameter R which monitors the intensity ratio of Raman scattering from a nonabsorbing solution, I_{TO}, to that from an absorbing solution, I_{obs}. I_{TO} is calculated by summing the contribution from each volume element with $\epsilon_0 = \epsilon_a = 0$. R monitors the degree to which absorption attenuates the Rayleigh- and Raman-scattered intensity. Thus, calculated values of R can be used to correct observed Raman spectra in order to obtain the Raman intensity values which would be observed in the absence of self-absorption:

$$I_{TO} = R(A_0, A_a, G) I_{obs} \quad (15)$$

where R is explicitly shown to depend upon the absorbances at the excitation wavelength, A_0, and at the scattered wavelength, A_a. The dependence of R upon the optical geometry is indicated by the parametric dependence upon G.

We limit the calculation presented here to a 90° scattering geometry with an approximately square collection optic and a cylindrical scattering volume uniformly illuminated by an excitation beam of uniform intensity along its cross section (Figs. 1–3). Other scattering geometries can easily be considered by changing the angle of incidence and the sample volume. We implicitly assume that the collection optic treats each volume element identically (i.e., large depth of focus and a large slit width and/or diffuse imaging). Our calculation does not include refraction of the scattered light which occurs upon entrance of the excitation beam into the sample and upon transmission of the scattered light out from the sample. Although refraction is easily included, it is ignored here since it is too sample-specific to be relevant to a general calculation. Refraction of the incident excitation would cause an increased convergence of the excitation beam within the sample, and the divergence of the scattered light would change as it left the sample. Refraction would lead to errors in the calculated absolute intensities which could be corrected for by renormalizing the solid angle intercepted by the collection optic.

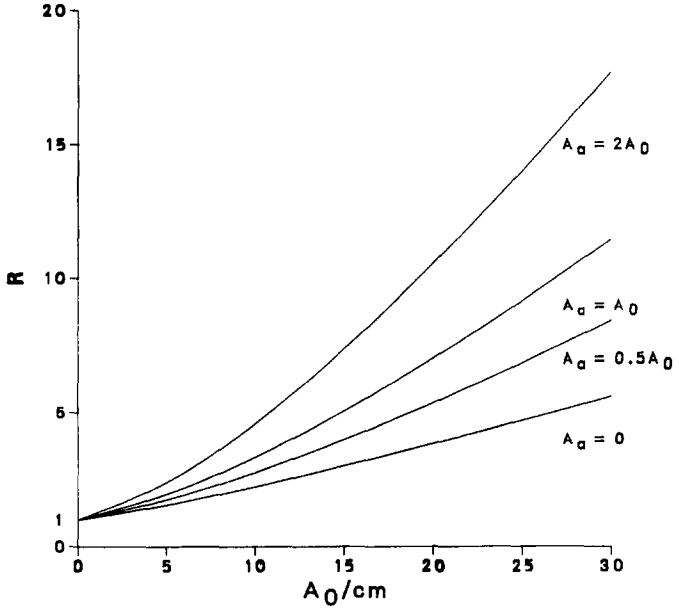

FIG. 6. The dependence of the self-absorption correction function R on the sample absorbances at the excitation (A_0) and Raman-scattered (A_a) wavelengths. $R = I_{TO}/I_{obs}$, where I_{TO} and I_{obs} are the Raman-scattered intensity from a nonabsorbing and absorbing sample, respectively. The calculation assumed a 1.0-mm-diameter capillary situated 10 cm from a 6-cm × 6-cm collection optic.

The self-absorption correction parameter was calculated with the use of the minimum number of volume elements in the 1.0-mm-diameter capillary required for convergence. Increasing the number of volume elements dramatically increases the calculation time. Larger sample absorbances require more volume elements for the calculation to converge. Table I clearly illustrates the fact that, even for a small sample of low absorbance, the scattering cannot be simply assumed to originate from an average single point located approximately at the center of the capillary.

RESULTS AND DISCUSSION

Figure 6 shows the dependence of the intensity ratio R on sample absorbances at the excitation wavelength, A_0, and the Raman- or Rayleigh-scattered wavelength, A_a. The plot for $A_a = 0$ shows attenuation associated with absorption of only the excitation light. For a cylindrical sample volume of 1.0 mm diameter and for sample absorbances at the excitation wavelength of 5, 10, 20, and 30/cm, we see that the Raman intensity decreases to 64%, 45%, 26%, and 18% of that which would be observed in the absence of absorption.

Previous self-absorption studies have simplified the self-absorption calculation by assuming that all of the Raman scattering derived from one average point within the sample. This approach is a poor approximation, even where only the excitation beam is absorbed. The Raman intensity would decrease to 56%, 32%, 10%, and 3% if all of the scattering derived from the center of the capillary for sample absorbances at the excitation wavelength of 5, 10, 20, and 30/cm, respectively ($A_a = 0$).

If the Raman-scattered light is also absorbed, the observed Raman intensity would further decrease. For example, if the absorbance at the Raman-scattered wavelength is identical to that at the excitation wavelength

TABLE II. The dependence of R upon sample absorbance at the laser excitation wavelength, A_0, and at the Raman band wavelength, A_a. See text for details.

	A_a				
A_0	0.0	5.0	10.0	20.0	30.0
0.0	1.00	1.27	1.57	2.27	3.06
5.0	1.56	1.95	2.39	3.37	4.49
10.0	2.24	2.76	3.33	4.58	5.92
20.0	3.84	4.59	5.37	7.03	8.77
30.0	5.60	6.51	7.46	9.42	11.43

($A_a = A_0$), the observed R values are 51%, 30%, 14%, and 8.7% for absorbances of 5, 10, 20, and 30/cm, respectively. Table II lists the value of R for various values of A_0 and A_a typical of those occurring in resonance Raman measurements of pure compounds and mixtures.

The decreased Raman intensities cause a decrease in the spectral signal-to-noise ratios and a corresponding increase in detection limits. The S/N ratio for a Raman measurement can be written:

$$\mathrm{S/N} = \frac{(I_a - I_B)}{(V_E + I_a + I_B)^{1/2}} \qquad (16)$$

where I_a is the analyte Raman intensity, I_B is the background intensity (which often derives from luminescence), and V_E is the variance of the electronic noise associated with the detector. The S/N ratio depends linearly on the analyte Raman intensity if the noise is dominated by detector electronic noise. As Table II indicates, an absorbance of 30 cm^{-1} for both the excitation and Raman-scattered light decreases the signal to 7% of that observed in the absence of absorption. In a low signal limit measurement, such as that with the use of intensified Reticon detector, the electronic noise dominates. Thus, the S/N ratio decreases to 7% of that which would occur in the absence of absorption, and the detection limit increases by a factor of fourteen. Thus, in the absence of strong resonance enhancement it is desirable to choose excitation wavelengths which minimize self-absorption. Self-absorption obviously cannot be avoided in resonance Raman measurements. However, the increased intensities associated with resonance enhancement generally more than make up for the self-absorption attenuation. Resonance enhancement scales approximately with the square of the molar absorptivity, while the self-absorption attenuation increases more gradually.

Since both the absorbance and the Raman-scattered intensity increase linearly with concentration, and because self-absorbance attenuates the observed intensity in a complex but exponential fashion, an optimum analyte concentration exists for resonance Raman measurements. Figure 7 shows a calculation of the Raman intensity which would be observed as a function of absorbance at the Raman-scattered and excitation wavelength. For absorption of only the exciting light we observe a saturation of the Raman intensity as the sample concentration increases. As the absorbance at the Raman-scattered wavelength increases, the intensity observed decreases, and a maximum appears at an absorbance of ~7/cm for $A_a = 2A_0$. For lower values of A_a, we see less distinct maxima shifted to higher values of A_0. The exact ordinate scaling of Fig. 7 is determined by the value of the incident excitation intensity and the analyte

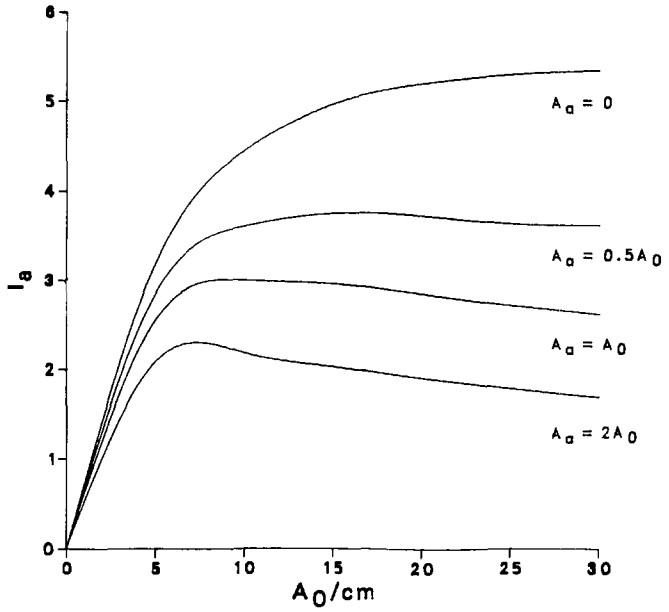

FIG. 7. Dependence of Raman intensity upon the sample concentration, assuming that all of the sample absorbance derives from the analyte. The optimal analyte concentration can be determined from $A_a = \epsilon_a c$.

Raman cross section. The position and prominence of the maximum depends only upon the sample absorbance.

Relative Raman intensity measurements are generally used both to determine Raman cross sections and concentrations of analyte.[10] Relative measurements are used because of the notorious difficulties involved in making absolute intensity measurements. The relative measurements utilize internal intensity standards whose Raman cross sections are known. Obviously, self-absorption biases these relative intensities if different absorbances occur at the wavelengths of the Raman bands of the analyte, compared to that of the internal standard. Thus, we have calculated the self-absorption correction factors required to correct these biased intensity ratios.

The magnitude by which self-absorption affects the relative Raman intensities has been calculated for the absorption band shape shown in Fig. 8A. The absorption band is Lorentzian, with a full width at half-maximum of 1000 cm^{-1}. Our results, shown in Fig. 8B, assume that excitation occurs at the edge of the absorption band exactly 1000 cm^{-1} below the maximum (at zero cm^{-1} on this arbitrary scale). Figure 8B shows the dependence upon absorbance of the relative ratios of intensities of analyte Raman bands to the intensity of a 1000-cm^{-1} internal standard band. The calculation assumes identical intensities for the analyte and internal standard bands in the absence of self absorption. The absicca indicates the maximum sample absorbance in the 1-mm-diameter sample capillary.

Since the absorbance for the 1000-cm^{-1} internal standard band is greater than for the analyte bands, the calculated relative ratios will be greater than one and will increase as the sample absorbance increases. Obviously, the ratio will be identical for bands symmetrically disposed about the absorption band maximum. The ratio is largest for the calculated bands at 0 cm^{-1} (Rayleigh scattering) and at 2000 cm^{-1}, and smallest for bands at 750 and 1250 cm^{-1}. The ratios increase less than lin-

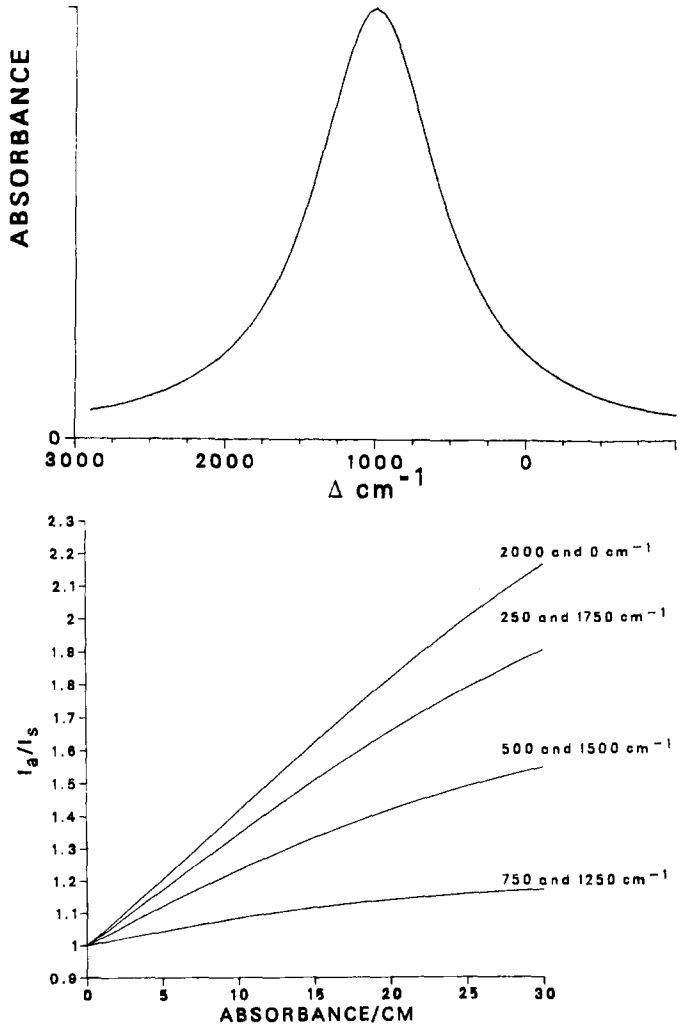

FIG. 8. The dependence upon self-absorption of the ratio of intensities of the analyte (I_a) and internal standard (I_s) Raman bands. (A) Absorption band: The absorption maximum occurs 1000 cm^{-1} from the excitation frequency. The full width at half-maximum for the absorption band is 1000 cm^{-1}. (B) Raman intensity ratio, as a function of sample absorbance. Laser excitation occurs at 0 cm^{-1}, while the internal standard band occurs at 1000 cm^{-1}, at the absorption maximum. The calculation assumes a 1.0-mm-diameter capillary situated 10 cm from a 6-cm × 6-cm collection optic.

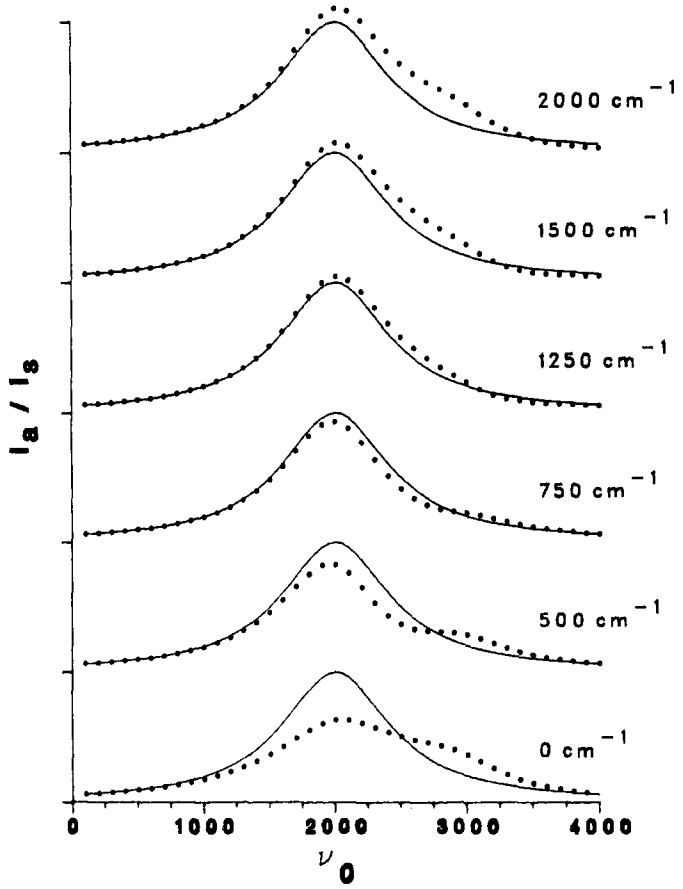

FIG. 9. Comparison between the actual and measured Rayleigh and Raman scattering excitation profiles from an absorbing sample. The Raman and Rayleigh bands have identical cross sections, and their actual excitation profiles exactly follow the absorption line shape, which is Lorentzian with a 1000 cm^{-1} full width at half-maximum and is centered at 2000 cm^{-1} on the arbitrary frequency axis shown. The calculation assumes a 1.0-mm-diameter capillary situated 10 cm from a 6-cm × 6-cm collection optic.

early as the absorbance increases. The relative intensity ratio for the 2000-cm^{-1} band is almost twice (1.87) the correct value when the sample absorbance at the internal standard band is 20/cm. These calculations clearly illustrate the potential bias that self-absorption can have on Raman relative intensity ratios.

Figure 9 shows the effect of self-absorption on measured relative intensity ratios in an excitation profile measurement through the absorption band illustrated in Fig. 8A. The internal standard band is Stokes shifted 1000 cm^{-1} from the excitation frequency ν_0. The calculation assumes identical cross sections for each of the bands and that the excitation profiles exactly follow the Lorentzian absorption band of Fig. 8A. This would occur, for example, when the absorption band shape is dominated by inhomogeneous broadening. The solid lines indicate the true shape of the excitation profiles. The influences of absorption on the relative intensity ratios for Rayleigh scattering (0 cm^{-1}), and Raman bands Stokes shifted 500, 750, 1250, 1500, and 2000 cm^{-1} from ν_0 are shown by the dots. The calculation assumes a maximum absorption of 20/cm and a 1.0-mm-diameter capillary illuminated by a collimated excitation beam of constant cross sectional intensity. A 6-cm × 6-cm square collection optic was situated 10 cm from the capillary. Contributions to Rayleigh scattering from the solvent were not included in the calculation. The Raman cross section of the internal standard was assumed to be constant throughout the absorption band, and we assume 100% efficiency for the collection optic, the spectrometer, and the detection system.

Figure 9 demonstrates that self-absorption has a dramatic effect on both the magnitude and the band shapes of the Raman excitation profiles. The lowest curve in Fig. 8, which shows the excitation profile for Rayleigh scattering, clearly displays the major biases which can occur for self-absorption; the excitation profile band becomes less pronounced and broader, and even shows an artifactual shoulder. The excitation profile data are little affected on the low-energy side, where little absorption of either the analyte or internal standard band occurs. However, as excitation occurs within the absorption maximum, the Rayleigh band is absorbed preferentially over the internal standard, which is Stokes shifted into a region of smaller absorption. Thus, the observed intensity ratio is decreased. As excitation occurs at higher energy

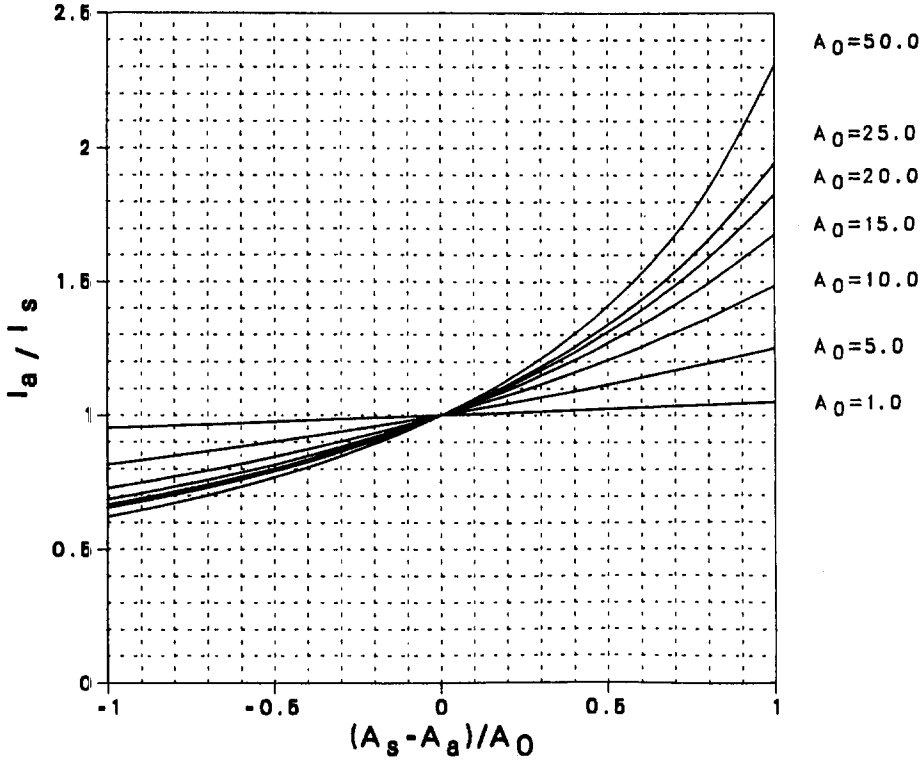

FIG. 10. The dependence of the self-absorption correction function on the difference in absorbances at the internal standard band, A_s, and Raman band wavelengths, A_a. The curves have been normalized to the absorbance at the incident laser wavelength, A_0. The self-absorption correction functions were calculated for 90° scattering from a 1.0-mm-diameter capillary situated 10 cm from a 6-cm × 6-cm square collection optic.

than the absorption band maximum, the internal standard band becomes preferentially absorbed and the observed ratio becomes larger than expected. Excitation at 2500 cm^{-1} is unique because the absorbances at the Rayleigh band and at the internal standard band are equal, and the observed ratio becomes identical to that which would occur in the absence of absorption.

Figure 9 shows that the detailed excitation profile band shapes of the analyte Stokes Raman bands depend on their separation from the internal standard band. The excitation profiles of bands with Raman shifts close to the internal standard band (750 cm^{-1} and 1250 cm^{-1}) are less affected by absorption processes than are bands widely separated from the internal standard band (500, 1500, and 2000 cm^{-1}). The difference in sample absorbance at the analyte and internal standard frequencies determines the magnitude of the deviation of the apparent relative ratios (dots) from the true relative ratios (solid lines).

The excitation profiles of Stokes bands with lower frequencies than the internal standard band appear narrower and slightly red-shifted from the true excitation profiles, and the apparent relative ratios are less than the true relative ratios when excitation is within the absorption band. As the excitation frequency increases, the internal standard band frequency passes through the absorption maximum. The shoulders on the high-frequency sides of the excitation profiles of the bands at 500 and 750 cm^{-1} are caused by selective attenuation of the internal standard band by self-absorption.

Raman excitation profiles of analyte bands at higher frequencies than that of the internal standard are broadened by self-absorption. The apparent relative ratios are larger than the true relative ratios, with excitation frequencies in resonance with the absorption band, because the internal standard band is closer to the absorption maximum than are the high frequency analyte bands. Excitation at frequencies above the absorption band maximum decreases the relative intensity ratio as the light scattered by high-frequency modes passes through the absorption maximum. The calculated intensity ratios for the 2000- and 1500-cm^{-1} bands with 4000-cm^{-1} excitation are below those of the true intensity ratios shown by the solid lines. Figure 9 clearly demonstrates that self-absorption may give artifactual structure in measured resonance Raman excitation profiles. These artifacts can be serious impediments in the analysis of excitation profile data. Obviously, if the absorption spectrum is structured, the potential artifacts must become more complex.

The effect of self-absorption on relative intensity ratios depends upon the absorbance difference at the analyte and internal standard bands, and on the absorbance at the excitation wavelength. Absorption of the exciting light by the sample preferentially increases the relative contributions of those volume elements closer to the collection optic and to the point of entrance of the beam. Figure 10 illustrates the dependence of the observed intensity ratio between an analyte and internal standard Raman band as a function of the difference in the internal standard band and analyte band absorbances ($A_s - A_a$). *This curve can be used directly to correct relative intensity excitation profile data for self-absorption, if the measurement geometry is similar to that used in this calculation.* The curves are normalized to the absorbance at the incident excitation wavelength, A_0.

These plots can be used to determine the self-absorp-

tion correction for any sample absorbances. For example, if the absorbance is 10/cm at the excitation wavelength and the absorbance at the internal standard Raman band is 5/cm greater than that of the analyte band, the observed intensity ratio will be artifactually increased by a factor of 1.2 due to self-absorption processes. Similarly, for an absorbance of 50/cm at the laser wavelength and a 25/cm larger absorbance at the internal standard wavelength than at the analyte wavelength, the observed ratio of intensities is 1.40 times higher than would be observed in the absence of self-absorption.

In general, sample absorbance differences between the analyte and the internal standard bands will be smaller than those chosen above, because the bands are relatively close in wavelength and because the absorption bands of condensed phase samples are relatively broad. Thus, the self-absorption corrections often encountered for samples with maximum absorbances as high as 20/cm are often below 20%. For a 90° scattering geometry, and a 1-mm cylindrical sample, the self-absorption correction for any sample absorbance may be accurately determined by interpolating between the plots shown in Fig. 10.

It should be noted that the calculations above are for linear absorption processes and must fail for high incident pulsed laser excitation where the absorption saturates. This is an uncommon situation in careful Raman measurements of ground-state species but can be important for Raman studies with pulsed laser sources.

As stated earlier, the calculation of self-absorption assumes that light originating anywhere within the illuminated portion of the capillary is equally likely to be imaged into the spectrometer. This is obviously incorrect for collection optics with small depths of focus. The calculation reported here is likely to be an overestimate of the exact self-absorption for the typical case of a high *f*/# lens; those volume elements towards the front of the capillary will generally be selected for optimum imaging, due to the fact that higher intensities originate from these volume elements. Thus, a small depth of focus will select volume elements that show less self-absorption attenuation.

SUMMARY

Correction parameters for self-absorption in resonance Raman and Rayleigh measurements have been calculated for the case of 90° scattering from a 1-mm-diameter cylindrical sample. We display curves that can be used to extract the correction factors, given the sample absorbances at the incident, analyte, and internal standard Raman wavelengths. Thus, observed Raman intensity ratios can be used to determine analyte concentrations and to calculate absolute Raman cross sections, as well as to determine excitation profiles from observed Raman intensity ratios.

ACKNOWLEDGMENTS

We gratefully acknowledge support of this work from NIH Grant 1R01GM30741-07. We would like to thank Peter Larkin for helping with the figures and Mike Falcetta for help with implementation of the software. Sanford A. Asher is an Established Investigator of the American Heart Association. This work was done during the tenure of an Established Investigatorship of the American Heart Association, Pennsylvania affiliate.

1. J. Behringer, in *Raman Spectroscopy, Theory and Practice*, H. A. Szymanski, Ed. (Plenum Press, New York, 1967), Vol. 1.
2. D. G. Rea, J. Opt. Soc. Am. **49,** 90 (1958).
3. F. Vratny and R. B. Fischer, Talanta **2,** 315 (1959).
4. F. Vratny, Anal. Chim. Acta **23,** 171 (1960).
5. J. S. Ard and H. Susi, Appl. Spectrosc. **32,** 321 (1978).
6. T. C. Strekas, D. H. Adams, A. Packer, and T. G. Spiro, Appl. Spectrosc. **28,** 324 (1974).
7. E. R. Lippincott, J. P. Sibilia, and R. D. Fischer, J. Opt. Soc. Am. **49,** 83, (1959).
8. D. F. Shriver and J. B. R. Dunn, Appl. Spectrosc. **28,** 319 (1974).
9. W. Rauch and H. Bettermann, Appl. Spectrosc. **42,** 520 (1988).
10. I. Tsukamnto, H. Nagai, and K. Machida, J. Raman Spectrosc. **17,** 313 (1986).
11. J. M. Dudik, C. R. Johnson, and S. A. Asher, J. Chem. Phys. **82,** 1732 (1985).
12. S. A. Asher, C. R. Johnson, and J. L. Murtaugh, Rev. Sci. Instrum. **54,** 1657 (1983).

Nondestructive Adhesive Analysis on Stamps by Fourier Transform Infrared Spectroscopy

MATTHEW POSLUSNY and KENNETH E. DAUGHERTY*
University of North Texas, Denton, Texas 76203

Spectroscopy has long been a popular subject with respect to postal stamps, but analysis of postal stamps has been the subject of only a few spectroscopic studies. Fourier transform infrared techniques were used in developing a nondestructive technique to analyze the adhesives on the back of stamps. This factor is of importance since the value of a stamp is partially dependent on the conditions of the original adhesive. Diffuse reflectance was finally settled on as the method of choice for this analysis, and it shows great promise not only for stamp analysis but also for other types of documentation analysis as well.

Index Headings: **Diffuse reflectance FT-IR; Adhesive analysis; Postal stamps.**

Received 31 May 1988.
* Author to whom correspondence should be sent.

INTRODUCTION

Spectroscopy has long been a popular subject with respect to postal stamps,[1,2] but analysis of postal stamps has been the subject of only a few spectroscopic studies. X-ray emission techniques have been used to detect forgeries, repairs, and misprints.[3,4] X-ray fluorescence has also been used to determine the precise color of stamps.[5]

We were interested in developing a nondestructive technique to analyze the backs of stamps, the adhesives, to determine whether these stamps had been reglued. This factor is important, since the value of a stamp is partially dependent upon the condition of the adhesive and also upon whether it is the original adhesive. Pre-

0003-7028/88/4208-1466$2.00/0